OPEN

Light: Science & Applications (2015) 4, e302; doi:10.1038/lsa.2015.75

www.nature.com/lsa

Original Article

An actively ultrafast tunable giant slow-light effect in ultrathin nonlinear metasurfaces

Cuicui Lu[1], Xiaoyong Hu[1,2], Kebin Shi[1,2], Qin Hu[1], Rui Zhu[1,2], Hong Yang[1] and Qihuang Gong[1,2]

A slow-light effect based on metamaterial-induced transparency (MIT) possesses great practical applications for integrated photonic devices. However, to date, only very weak slow-light effects have been obtained in metamaterials because of the intrinsic loss of metal. Moreover, no active control of slow-light has been achieved in metamaterials. Here, we report the realization of a giant slow-light effect on an ultrathin metasurface that consists of periodic arrays of gold nanoprism dimers with a thickness of 40 nm sandwiched between a multilayer-graphene micro-sheet/zinc oxide nanoparticle layer and a monolayer graphene/polycrystalline indium tin oxide layer. The strong field confinement of the plasmonic modes associated with the MIT ensures a tremendous reduction in the group velocity around the transparency window. A group index of more than 4×10^3 is achieved, which is one order of magnitude greater than that of previous reports. A large tunable wavelength range of 120 nm is achieved around the center of the transparency window when the pump light intensity is only 1.5 kW cm^{-2}. The response time is as fast as 42.3 ps. These results demonstrate the potential for the realization of various functional integrated photonic devices based on metasurfaces, such as all-optical buffers and all-optical switches.
Light: Science & Applications (2015) **4,** e302; doi:10.1038/lsa.2015.75; published online 19 June 2015

Keywords: graphene; metamaterial-induced transparency; metasurfaces; slow light effect; Zno nanoparticles

INTRODUCTION

The slow-light effect plays an essential role in the field of nonlinear optics. Typical materials that have been used to achieve the slow-light effect include photonic crystals, optical fibers, and optical microcavities.[1–5] Recently, the slow-light effect has been realized based on metamaterial-induced transparency (MIT).[6–11] However, only a small group index of 100 was obtained in photonic metamaterials because of the relatively large intrinsic loss of metal.[6–11] Moreover, various functional integrated photonic devices, including ultrafast all-optical buffers and all-optical switches, require ultrafast control of the slow-light effect. Photonic metasurfaces offer a variety of opportunities to control light using flat and surface components and have attracted wide attention for their great practical applications in the field, such as optical computing, optical communications, and integrated photonic circuits.[12–17] To date, no ultrafast active control of the slow-light effect in metamaterials has been reported.

In this letter, we report the realization of an ultrafast all-optical tunable giant slow-light effect in an ultrathin metasurface. The metasurface consists of periodic arrays of gold nanoprism dimers sandwiched between a multilayer-graphene micro-sheet/zinc oxide (ZnO) nanoparticle layer and a monolayer graphene/polycrystalline indium tin oxide (ITO) layer. The strong field confinement of the plasmonic modes associated with the MIT ensures a large reduction in the group velocity in the transparency window. The enhanced nonlinearity brought about by the quantum confinement (QC) effect provided by the ZnO nanoparticles and polycrystalline ITO nanograins, hot electron injection from the gold nanoprism to monolayer graphene, and reinforced interaction between the light and matter provided by the multilayer-graphene micro-sheets ensures a very large nonlinear refractive index for the metasurface sample. Therefore, ultralow power for the all-optical tunability can be obtained relative to previously reported all-optical tunable metamaterials.[6,18–21] This study not only provides a scheme to construct large optical nonlinear photonic materials with ultrafast response but also provides opportunities for the realization of low-power ultrafast photonic devices for integration based on metasurfaces.

MATERIALS AND METHODS

The fabrication process of the metasurface sample is shown in Figure 1a. First, a monolayer of graphene was covered on the surface of an ITO film (180-nm-thick) on a SiO_2 substrate using chemical vapor deposition (CVD). Second, periodic arrays of gold nanoprism dimers were patterned on the surface of the monolayer graphene through an electron-beam lithography (EBL) system. Figure 1b shows the three-dimensional structure of one gold nanoprism dimer unit. Third, ZnO nanoparticles were covered on the surface of the periodic arrays of gold nanoprism dimers by using the spin coating method. Fourth, multilayer-graphene micro-sheets were covered on the surface of the ZnO nanoparticle layer. The details of the sample fabrication are provided in the supplementary information. The left nanoprism was arranged handstand-like, and the right nanoprism erect, as shown in Figure 1b. A top-view scanning electron microscopic (SEM) image of the plasmonic crystal of gold nanoprism dimers with a square lattice is presented in Figure 1c. The period was 1000 nm. Both of the nanoprisms took on the configuration of an equilateral triangle with a lateral

[1]State Key Laboratory for Mesoscopic Physics & Department of Physics, Peking University, Beijing 100871, China; and [2]Collaborative Innovation Center of Quantum Matter, Beijing 100871, China
Correspondence: XY Hu, Email: xiaoyonghu@pku.edu.cn
Received 20 October 2014; revised 25 February 2015; accepted 12 March 2015; accepted article preview online 16 March 2015

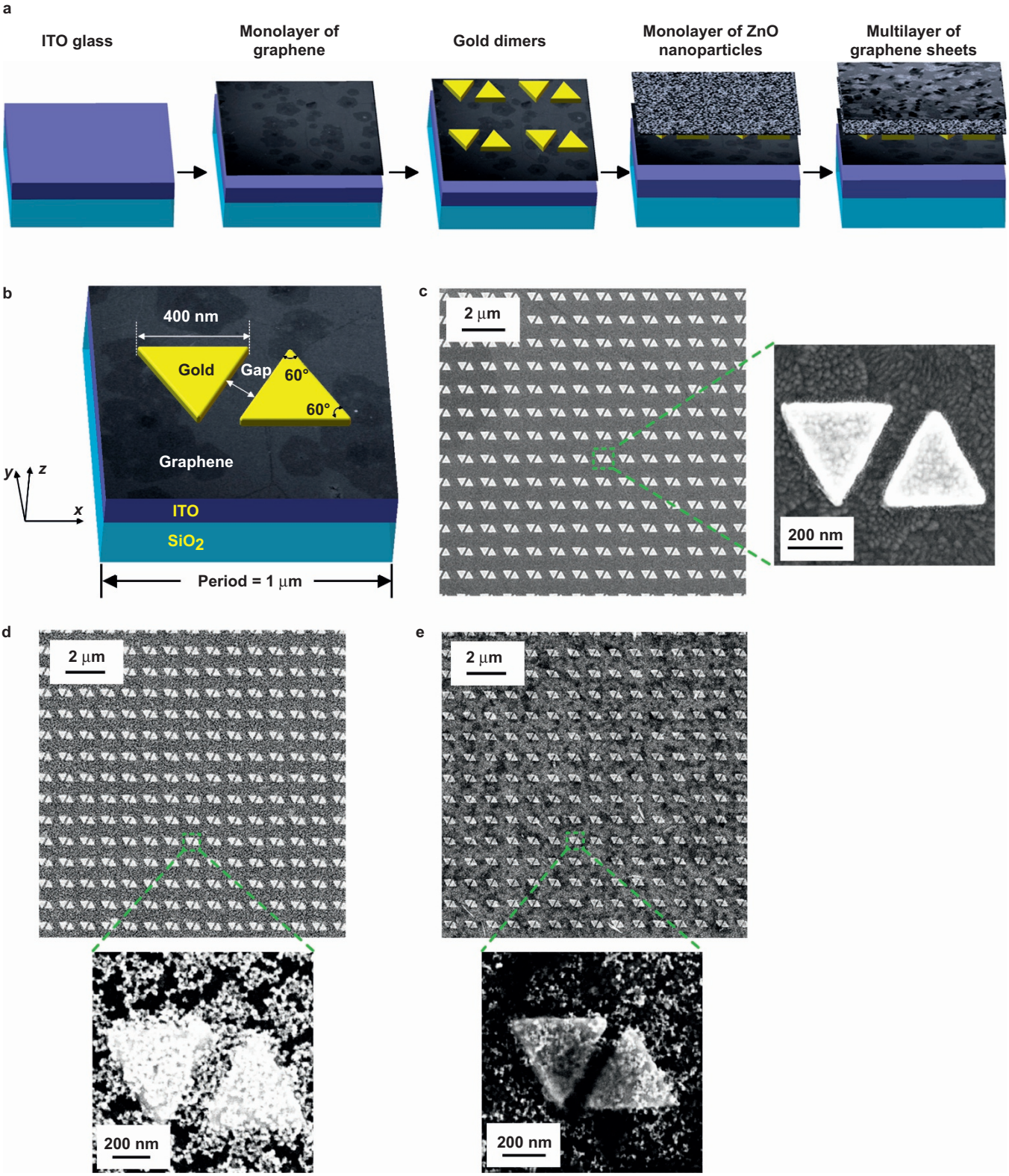

Figure 1 Characteristics of the metasurface structures. (**a**) Fabrication process. (**b**) Three-dimensional schematic structure of a gold nanoprism dimer in one unit cell without ZnO nanoparticles and multilayer graphene on the gold nanostructures. Top-view SEM images at low and high magnification of the metasurfaces without ZnO nanoparticles and multilayer graphene (**c**), with ZnO nanoparticles (**d**), and with ZnO nanoparticles and multi-layer graphene micro-sheets (**e**). The insets with the green arrows pointing at them are small-scale images for (**c**), (**d**), and (**e**).

doi:10.1038/lsa.2015.75

length of 400 nm. Both the length and the width of the entire patterned area were 300 μm. The ITO film took on a polycrystalline configuration, consisting of crystal nanograins (the average diameter was less than 30 nm), clearly shown in the inset of Figure 1c. The average size of the ZnO nanoparticles on the gold dimer array was approximately 10 nm, as seen from the inset in Figure 1d. The ZnO nanoparticles were homogeneously distributed to form a ZnO dielectric layer. The multilayer-graphene micro-sheets cover layer consisted of a mixture of 70% thin sheets (from 1 to 10 layers) and 30% thick sheets (from 11 to 30 layers). The black regions in Figure 1e correspond to the thick multilayer-graphene micro-sheet regions, and the white regions are the thin multilayer-graphene micro-sheet regions.

RESULTS AND DISCUSSION

The transmission spectrum of the samples was measured using an optical micro-spectroscopy system (see supplementary information). We first measured the linear transmission properties of the metasurface without the multilayer-graphene micro-sheet/ZnO nanoparticle cover layer (Figure 2a). The transmission shown is the normalized results, which is the ratio of the transmission for the sample with meta-structures to that of a pure gold film (40-nm-thick) coated on an ITO film (180-nm-thick) on a SiO_2 substrate.[6,22] The absolute intensity of the probe light propagating through the metasurface sample was more than 20 000 a.u., whereas that of the reference film was more than 45 000 a.u. There was a narrow transparency window within the wide forbidden band, which indicates the formation of the MIT. A high transmission of 80% was maintained in the center of the transparency window. The width of the transparency window was reduced with the increase of the gap distance between the two gold nanoprisms, i.e., when the gap distance was 52 nm, 104 nm, and 156 nm, the corresponding full-width of the half-maximum of the transparency window was 348 nm, 301 nm, and 298 nm, respectively. This is mainly the result of the difference in coupling strengths between the dark modes and bright modes brought about by different gaps. The measured results agree with the calculated results in Figure 2b, except that the position of the two dips exhibits a very large discrepancy between theory and experiment, i.e., the measured MIT linewidths are significantly broader than the calculated linewidths. The reasons for this discrepancy can be understood as follows: first, the gold nanoprisms took on a polycrystalline configuration composed of nanoscale gold grains with an average diameter of 4 nm, as shown in Figure 1c and Figure S9 in the Supplementary Information. This results in a rough surface of gold nanoprisms. Second, the gold nanoprisms were not perfectly etched. For example, the vertexes of the gold nanoprisms were round, and the edges of the gold nanoprisms were curved. Yurista *et al.* and Davis *et al.* noted that the rough surfaces of metamolecules and imperfectly fabricated metamolecules will add additional losses, which will broaden the bandwidth of the transparency window of the MIT and reduce its transmission.[23–26] This broadened bandwidth has been confirmed by Nau's measurements.[27] The average surface roughness of the ZnO and ITO films were approximately 5 nm and 45 nm, respectively, as shown in Figure 1c and Figure S9 in the Supplementary Information. It is the transparency window center that determines in which wavelength the maximum slow-light effect can be found. The measured central wavelength of the transparency window of the MIT, 1300 nm, was in agreement with the calculated central wavelength. The very large discrepancy between the calculated and measured positions of the two dips has no influence on the study of the slow-light effect. To elucidate the physical mechanism for the MIT, we calculated the electric field distributions and current density distributions of the gold nanoprism dimers with a gap of 104 nm. Figure 2c–2e shows the calculated Y-polarized electric field distributions for different incident wavelengths of 1260 nm (located in the first transmission valley of the MIT), 1300 nm (in the transparency window peak), and 1400 nm (in the second transmission valley of the MIT), respectively. The bright modes can be excited directly by the incident weak electric field, whereas the dark modes can only be excited by the coupling of the bright modes. The interference between the dark mode and bright mode generates MIT. For the 1260 nm and 1400 nm incident light, the electric field distributions were strong in each corner of the nanoprisms (as shown in Figure 2c and 2e), which demonstrates that strong bright modes are excited, whereas for the 1300 nm incident light (Figure 2d), the field distributions were weak at the adjacent sides of the two nanoprisms, which demonstrate the destructive interference caused by the strong coupling of the dark modes and the bright modes.[7,24] From the calculated current density distribution, it is easy to find that for the 1260 nm and 1400 nm incident light, the electric dipole modes (bright modes) are excited, and the current density in the gap area for the adjacent two nanoprisms has the same sign (Figure 2f and 2h), which takes on an ''antibonding'' configuration. By contrast, for the 1300 nm incident light, the electric quadrupole modes (dark modes) are excited due to the bright modes coupling, and the current density in the gap area for the adjacent two nanoprisms has the reverse sign (as shown in Figure 2g), which takes on a ''bonding'' configuration. In a manner analogous to atom energy-level splitting, the ''antibonding'' configuration has a higher energy level than the ''bonding'' configuration, and therefore the ''antibonding'' corresponds to the superradiance and ''bonding'' corresponds to the subradiance.[11,24] Biswas *et al.* noted that the electric field distributions of different dipole plasmonic modes is different even though they may have similar current density distributions.[11]

To investigate the slow-light effect brought about by MIT, we first calculated the linear transmission spectrum and group refractive index of the metasurfaces with different gap distances for the gold nanoprism dimer unit, which is shown in Figure 3a and 3b. The group refractive index was not directly obtained from the transmission spectrum (the detailed calculation methods are shown in the Supplementary Information). Zhao *et al.* demonstrated that the phase shift of incident light propagating through a metasurface was solely determined by the surface plasmon response, and the influence of multiple reflections of light through the metasurface can be neglected.[28] As shown in Figure 3a, a distinct MIT effect was obtained in the metasurfaces. The wider the gap, the narrower the linewidth of the transparency window. The group refractive index n_g was calculated to be 4×10^3 at 1300 nm for the metasurface sample with a gap distance of 104 nm between the two gold nanoprisms, as shown in Figure 3b. We also calculated, using the finite element method, the pass time of a Gaussian laser pulse (with a wavelength of 1300 nm and a pulse duration of 35 fs) through the metasurface sample under conditions in which the pulse does not have excessive aberration. The pass time was delayed by 500 fs compared with that through the air, confirming that a very large group index of 4×10^3 was obtained for the metasurface. The group refractive index increased from 2.7×10^3 to 7.7×10^3 around the transparency window when the gap distance increased from 9 nm to 199 nm, which can be understood from the underlying physical mechanism of MIT. Analog to the three-level atom system, the linear response of a meta-atom to resonant light can be described using the first-order susceptibility χ. The real part of the susceptibility $\mathrm{Re}[\chi]$ determines the refractive index, whereas its

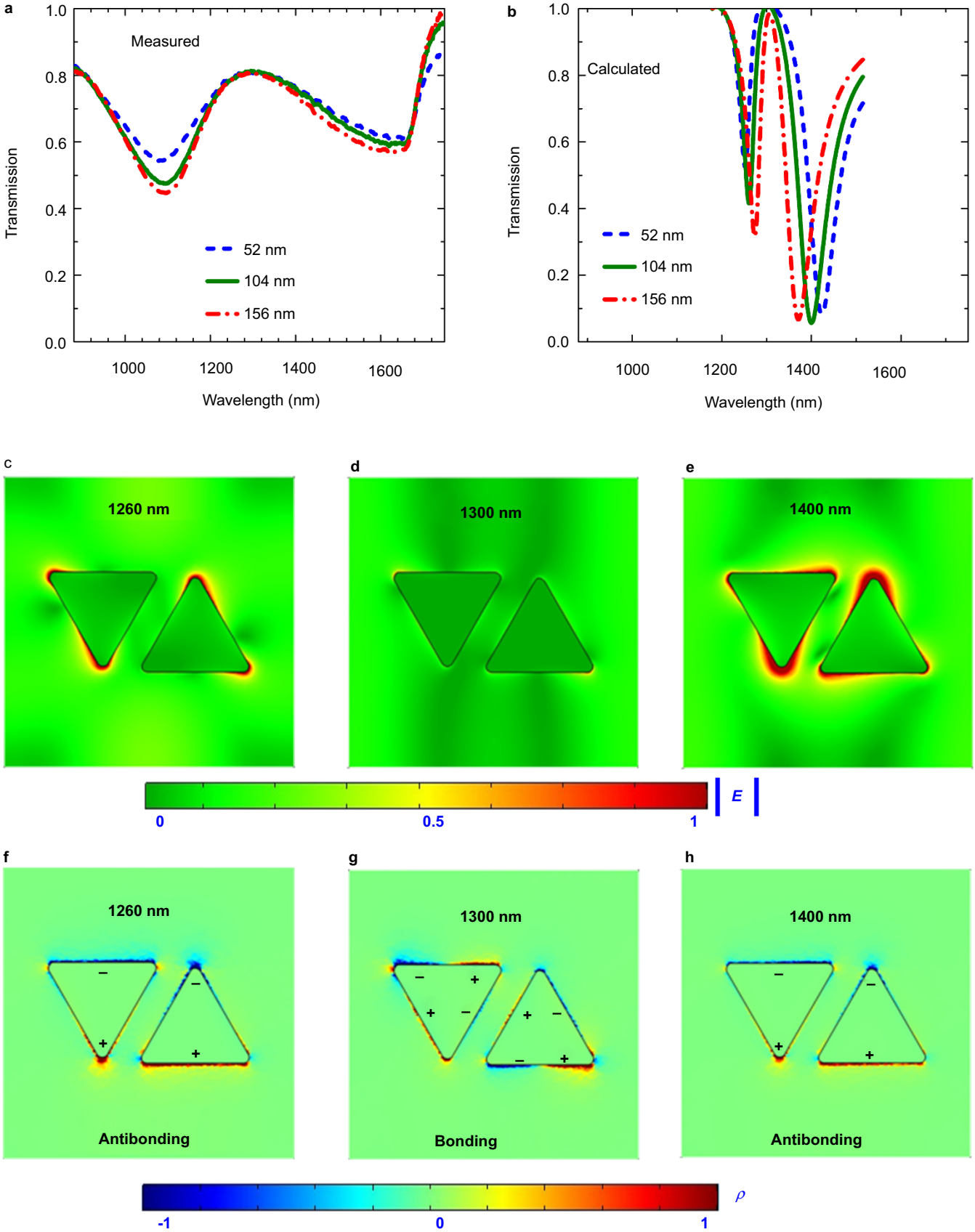

doi:10.1038/lsa.2015.75

Figure 2 Linear transmission spectrum measurements and calculations for MIT. (**a**) Measured transmission spectra of the metasurface with different gaps. (**b**) Calculated transmission spectra of the metasurface with different gaps between the two gold nanoprisms of 52 nm (blue dotted), 104 nm (green solid), and 156 nm (red dash dotted), All the incident cases were set to be Y-polarized. Electric-field distributions (**c–e**) and current-density distributions for the component in the *Y* direction (**f–h**) on the upper surface of the gold dimers with different incident wavelengths. (**c**) and (**f**): λ = 1260 nm; (**d**) and (**g**): λ = 1300 nm; (**e**) and (**h**): λ = 1400 nm. The legends for the magnitudes of the electric field and current density are normalized.

imaginary part Im[χ] determines the field dissipation.[7] Considering the case of a small detuning and the second-order approximation, the susceptibility can be written as[7,10]

$$\chi \propto \delta \frac{\kappa^2 - \gamma_b^2}{(\kappa^2 + \gamma_a\gamma_b)^2} + i\frac{\gamma_b}{\kappa^2 + \gamma_a\gamma_b} + i o(\delta^2) \quad (1)$$

where κ is the coupling between the bright atom and the dark atom, δ is the detuning of the atom resonance frequency and the incident light frequency, and γ is the damping factor of atom. For strong coupling, $\kappa >> \sqrt{\gamma_a\gamma_b}$, so we have $\chi \propto 1/\kappa^2$. The wider the gap, the weaker the coupling strength between the bright atom and the dark atom. This indicates that κ decreases with the increase of the gap, which leads to a increment in Im[χ], corresponding to an enlarged absorption cross-section of the meta-atom σ. Fleischhauer *et al.* noted that the linewidth of the transparency window $\Delta\lambda$ satisfies the relation[7]

$$\Delta\lambda \propto \frac{1}{\sqrt{\sigma}} \quad (2)$$

It is very clear that the linewidth of the transparency window $\Delta\lambda$ decreases with the increase of the gap. Moreover, the Im[χ] is increased due to the decrease of κ, so the transmission of the transparency window is decreased due to the increased loss (see Figure 2a). Tassin *et al.* showed that the stronger the excitation of the dark plasmonic mode using the bright plasmonic mode, the larger the group index is, due to the more intense destructive interference between the bright and dark modes.[29] The excitation ζ of the dark plasmonic mode can be estimated by the relation[29]

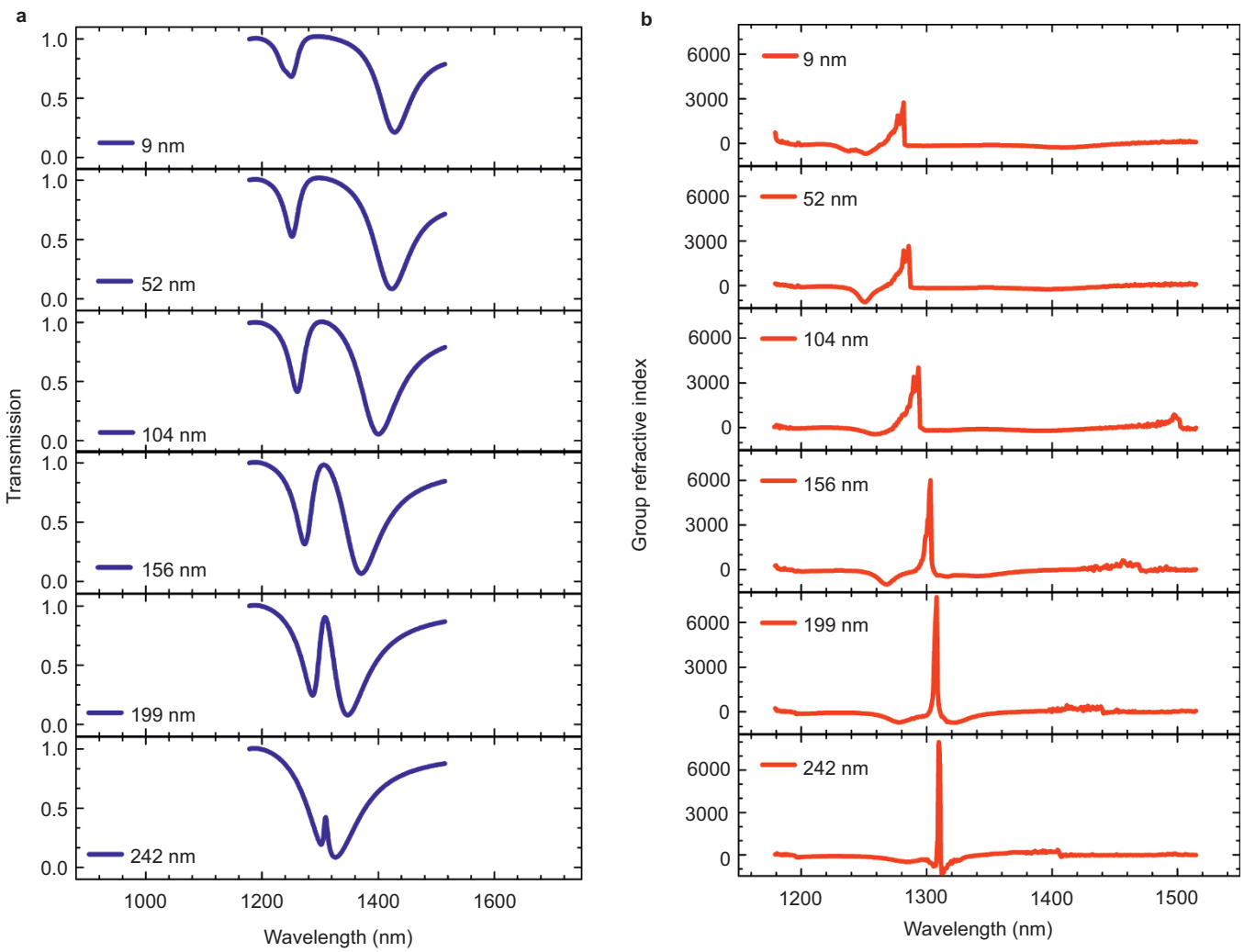

Figure 3 Calculated transmission spectrum (**a**) and group refractive index (**b**) for the metasurface with different gap distances for the gold nanoprism dimer unit. The gap distances between the two gold nanoprisms are 9 nm, 52 nm, 104 nm, 156 nm, 199 nm, and 242 nm.

$$\zeta \propto \frac{1}{\kappa} \quad (3)$$

Therefore, a weak coupling between the bright and dark modes leads to a stronger excitation of the dark modes, and subsequently, a larger group refractive index can be obtained. For a larger gap, the coupling between the bright and dark modes was weakened, which results in an enlarged group refractive index. This has been confirmed by the measurements of Tassin *et al.*[29] According to our design, the largest gap can be set to 260 nm, because the period is 1000 nm; if the gap is more than 260 nm, the adjacent dimer pair has less gap distance, so the group refractive index will decrease. Hence, the maximum group refractive index for the gold nanoprism dimer is slightly more than 7.7×10^3, so the corresponding MIT has a smaller transmission around the transparency window. In fact, with the further decrease of the gap, it is no longer the real "MIT" but rather the Autler-Townes (AT) splitting, which only looks similar to "MIT" with a broader transparency window due to the strong coupling (see the top figure in Figure 3a).[30,31] The smaller the gap, the larger detuning of the two resonances, which results in the generation of AT, and that is why the "MIT" has a large transparency window when the gap is 9 nm or smaller. The acquisition of the giant group index in an ultrathin metasurface may results from three aspects. First, the gold nanoprism has stronger localization due to its sharper corner compared to a cuboid;[10,11] second, the variety of modes existing in the gold nanoprism makes coupling between the two nanoprisms much easier;[32] third, if the plasmonic microstructure is compared with the "optical microcavity", it is easy to see that the quality factor value ($Q \propto 1/\Delta\omega$) increases with the decrease of the linewidth of the transparency window brought about by the increased gap distance, as shown in Figure 3b, i.e., the photon lifetime increase corresponds to the strengthened slow-light effect.[33,34] We also investigated the dependence of the MIT lineshapes on the structural parameters, including the period of the dimers, the lateral length of the nanoprisms, the thickness of the gold nanoprisms, and different incident polarizations (detailed in the Supplementary Information). It was found that the MIT lineshape has an obvious red-shift with the increase of the period, whereas the lateral length and the gold thickness have little influence on the MIT. With the polarization change, the MIT lineshape experiences a great change due to the great coupling changes of the bright modes.

An optical interference experiment was performed to characterize the slow-light time. The all-optical tunability of the metasurface was also demonstrated by an interference experiment setup by varying the pump intensity. The sample had a gap distance of 104 nm for the gold nanoprism dimer unit and an effective thickness of 40 nm for the slow-light effect. The schematic experimental setup is depicted in Figure 4a (see Supplementary Information for detailed setup and measurements), which has a Mach–Zehnder interferometer configuration. The incident probe beam was Y-polarized and was focused to approximately 100 μm. When the pump laser was switched off, perfect interference fringes were obtained for two probe pulses propagating through two identical 180-nm-thick ITO films on SiO_2 substrates at zero time delay for different probe wavelengths (as shown in Figure 4b), because the optical path difference was zero. When one 180-nm-thick ITO film on SiO_2 substrate was replaced by the metasurface sample, perfect interference fringes were obtained at a time delay of 500 fs when the incident wavelength was 1300 nm (see Figure 4c). A very large group index of 4×10^3 was obtained for the metasurface sample, one order of magnitude larger than those of previous reports.[6–11] Under the excitation of a 1.5 kW cm^{-2} pump laser (λ = 1300 nm), only when the probe wavelength was reduced to 1180 nm could the interference fringes be obtained under the same time delay of 500 fs, as shown in Figure 4d. The effective refractive index of the multilayer-graphene micro-sheet/ZnO nanoparticle layer and the monolayer graphene/polycrystalline ITO layer was decreased, resulting from the optical Kerr effect under the excitation of the pump laser.[35,36] Accordingly, the plasmonic modes provided by the gold nanoprism dimers have a blue-shift, and the transparency window has a blue-shift. To further verify the measured time delay, we calculated the transmission spectrum of the metasurface sample under different pump intensities. The transmission spectrum has a blue-shift resulting from the negative large nonlinear refractive index of the multilayer-graphene micro-sheet/ZnO nanoparticle layer and the monolayer graphene/polycrystalline ITO layer (see Figure 4f). If we still used the 1300-nm probe light when the 1.5 kW cm^{-2} pump laser was switched on, the interference fringes would be obtained at approximately t = 0.3 fs due to the increased optical path brought about by the ZnO layer and multilayer graphene relative to pure ITO glass, as shown in Figure 4e. Figure 4g shows the measured time delay to obtain perfect interference fringes for a 1300-nm-probe laser under different pump laser intensities. The time delay changes from 500 fs to 0.3 fs to obtain perfect interference fringes upon increasing the pump laser intensity from 0 to 1.5 kW cm^{-2}. This demonstrates that the slow-light effect can be continuously tuned within a wavelength range of 120 nm. Thus, we can freely modulate the slow-light effect by using a pump laser. If more identical metasurface samples are cascaded, an optical buffer with a large delay time can be realized. For example, a large time delay on the order of several hundred picoseconds can be achieved by cascading many layers of metasurfaces. The delay-bandwidth product was calculated to be 42.3 for the metasurface,[37] which confirms that the metasurface has potential applications in slow-light signal processing devices. A possible way to solve the problem of losses is to add a transparent gain medium under or above the metasurface.[9,10]

To confirm the all-optical tunability, the transmission changes of the 1180-nm-probe light were measured using an optical pump-probe experimental setup (see Supplementary Information). Figure 5a shows that the intensity was 1.5 kW cm^{-2} and 0.1 kW cm^{-2} for the pump and probe pulses, respectively. The probe wavelength was located at the maximum slope between the first valley and the transparency peak of the MIT (see Figure 2a). At first, the transmission was 61% for the probe light, but it increased to 78% when the pump and probe pulses overlapped, which indicates that the transparency window has a blue-shift resulting from the negative nonlinear refractive index of the multilayer-graphene micro-sheet/ZnO nanoparticle layer and the monolayer graphene/polycrystalline ITO layer.[35,36] This is confirmed by the calculated transmission spectrum (Figure 4f) of the metasurface sample under the excitation of a 1.5 kW cm^{-2} pump laser. Thus, a tunable wavelength range of up to 120 nm was realized for MIT. The dynamic transmission change in the drop process of Figure 5a reflects the response time of the all-optical tunability. We used an exponential fit to characterize the response time to the measured data (see the red line of Figure 5a). In the fast process, the time constant was measured to be 1.96 ps, and in the relatively slow process, the time constant was measured to be 42.3 ps. The ultrafast response of the fast process, 1.96 ps, was determined by the third-order optical nonlinear response of graphene.[38] The ultrafast time response of τ_2 is mainly caused by the relaxation of the third-order nonlinear response of gold nanoparticles and hot electron injection from the gold

doi:10.1038/lsa.2015.75

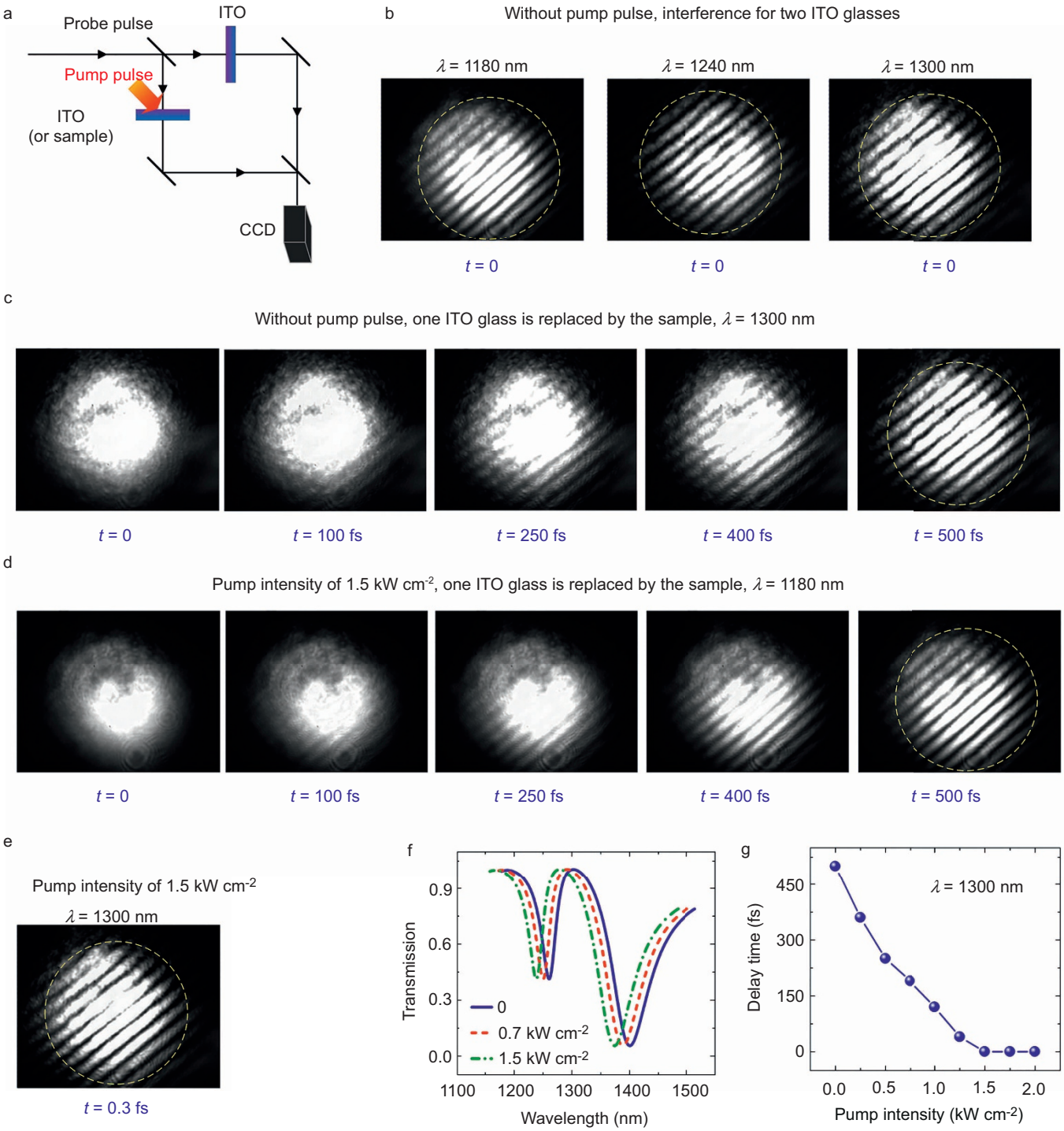

Figure 4 Measured time delay and dynamic tuning for slow-light on the metasurface. (**a**) Schematic experimental setup for the time delay measurement of slow-light. (**b**) CCD images for the interference of two probe pulses split through two ITO glasses. The incident wavelengths were 1180 nm, 1240 nm, and 1300 nm, corresponding to numbers of interference fringes of 10, 10.5, and 11, respectively. One ITO glass was replaced by the sample for (**c**), (**d**), (**e**), and (**f**). (**c**) CCD images for the interference of two probe pulses (λ = 1300 nm, where n_g = 4026) at different times by adjusting the delay line without the pump pulse. The number of interference fringes is 11 (shown in the yellow dotted circle). (**d**) CCD images for the interference of two probe pulses (λ = 1180 nm) at different times by adjusting the delay line with a pump pulse of 1180 nm. The maximum value of n_g has a blue-shift due to the third-order nonlinear effects. The number of interference fringes is 10 (shown in the yellow dotted circle). (**e**) CCD images for the interference of two probe pulses (λ = 1300 nm) with a pump pulse of 1180 nm. The maximum value of n_g has a blue-shift due to the third-order nonlinear effects. (**f**) Calculated transmission spectrum for different pump intensities. (**g**) Measured delay time change by increasing the pump laser intensity for λ = 1300 nm. CCD, charge coupled device.

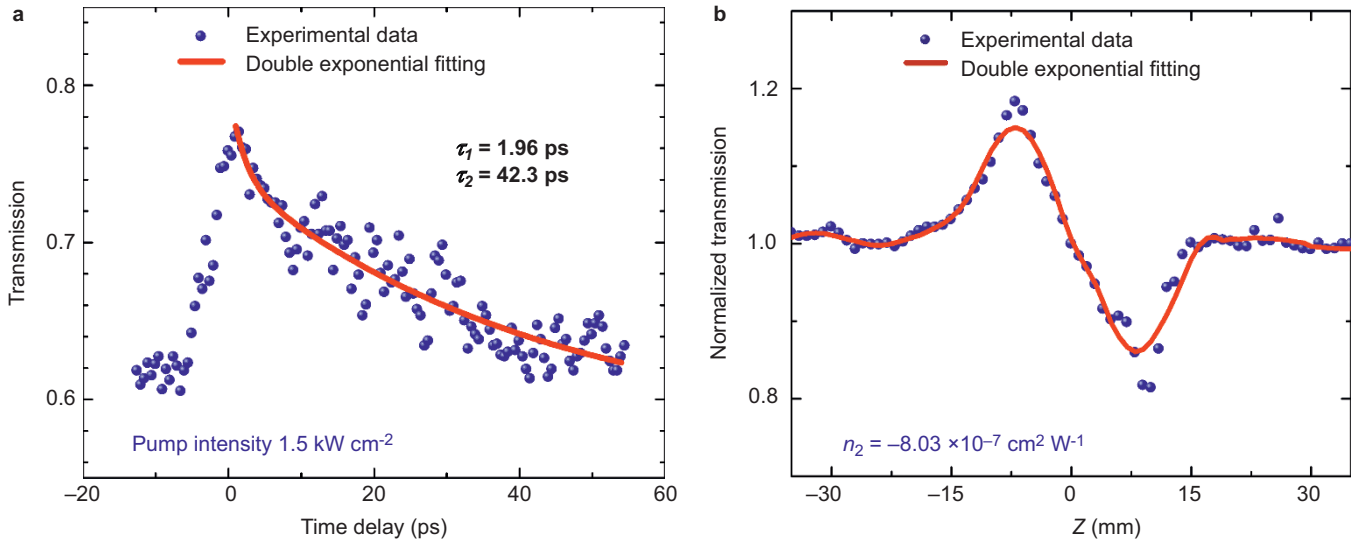

Figure 5 (**a**) Measured time delay between the pump and probe pulses with a wavelength of 1180 nm. The time constant was obtained from an exponential fit of the data of the red line. (**b**) Measured n_2 for the layer of ZnO-nanoparticles/multilayer graphene micro-sheets by adopting a closed-aperture Z-scan scheme.

nanoprism to ITO.[39–41] To further confirm the ultra-low power all-optical tunability, we adopted a closed-aperture Z-scan scheme to measure the effective three-order nonlinear refractive index n_2 of the film composed of ZnO nanoparticles and multilayer-graphene micro-sheets (Figure 5b).[42] The measured result for the effective nonlinear refractive index n_2 was -8.03×10^{-7} cm^2 W^{-1}. Compared with the conventional material of silicon (n_2 is -3.16×10^{-14} cm^2 W^{-1}), our metamaterial is seven orders of magnitude greater in the near-infrared range.[43] We also measured n_2 for an ITO film with monolayer graphene and an ITO film with a monolayer and ZnO nanoparticles (Supplementary Information Fig. S8) and found that the film composed of ZnO nanoparticles and multilayer-graphene micro-sheets has the larger n_2. The large nonlinear refractive index of the metasurface sample is attributed the following aspects. The tremendously enlarged thickness of the multilayer-graphene micro-sheets results in exceedingly enhanced interaction between light and graphene compared with monolayer graphene.[21,44] Moreover, the small size of 800-nm multilayer-graphene micro-sheets and the inhomogeneous surface limit the diffusion of carriers and increase the carrier density per volume. By contrast, ZnO nanoparticles and ITO nanograins have excellent third-order nonlinearity due to quantum size confinement effects on the intensity (Supplementary Fig. S9). The hot electron injection from the gold nanoprisms to the ITO film also provides an important interaction path for nonlinearity.[41] The threshold pump intensity of 1.5 kW cm^{-2} is more than six orders of magnitude lower than those of previous reports.[6] Therefore, an ultralow pump power was achieved.

CONCLUSIONS

We have achieved an ultrafast and ultralow-power all-optical tunable giant slow-light effect in an ultrathin metasurface. A large group index of more than 4×10^3 was obtained. Under the excitation of an ultralow pump laser of 1.5 kW cm^{-2}, the transparency window shifted up to 120 nm. The response time was as fast as 42.3 ps. This work not only opens possibilities for the realization of ultrafast optical buffers in the field of integrated photonic chips but also offers strategies for constructing large nonlinear photonic materials with ultrafast response.

ACKNOWLEDGEMENTS

This work was supported by the 973 Program of China under grant nos. 2013CB328704 and 2014CB921003, the National Natural Science Foundation of China under grant nos. 11225417, 61475003, 11134001, 11121091, and 90921008. We thank QQ Gan of the State University of New York at Buffalo for the helpful discussions.

1 Vlasov YA, O'Boyle M, Hamann HF, McNab SJ. Active control of slow light on a chip with photonic crystal waveguides. *Nature* 2005; **438**: 65–69.
2 Gersen H, Karle T, Engelen R, Bogaerts W, Korterik J *et al.* Real-space observation of ultraslow light in photonic crystal waveguides. *Phys Rev Lett* 2005; **94**: 073903.
3 Song KY, Herráez MG, Thévenaz L. Observation of pulse delaying and advancement in optical fibers using stimulated Brillouin scattering. *Opt Express* 2005; **13**: 82–88.
4 Sharping JE, Okawachi Y, Gaeta AL. Wide bandwidth slow light using a Raman fiber amplifier. *Opt Express* 2005; **13**: 6092–6098.
5 Lee JY, Fauchet PM. Slow-light dispersion in periodically patterned silicon microring resonators. *Opt Lett* 2012; **37**: 58–60.
6 Gu JQ, Singh R, Liu X, Zhang XJ, Ma YF *et al.* Active control of electromagnetically induced transparency analogue in terahertz metamaterials. *Nat Commun* 2012; **3**: 1151.
7 Fleischhauer M, Imamoglu A, Marangos JP. Electromagnetically induced transparency: Optics in coherent media. *Rev Mod Phys* 2005; **77**: 633–673.
8 Husko C, Vo TD, Corcoran B, Li J, Krauss TF *et al.* Ultracompact all-optical XOR logic gate in a slow-sight silicon photonic crystal waveguide. *Opt Express* 2011; **19**: 20681–20690.
9 Sandtke M, Kuipers L. Slow guided surface plasmons at telecom frequencies. *Nat Photonics* 2007; **1**: 573–576.
10 Zhang S, Genov DA, Wang Y, Liu M, Zhang X. Plasmon-induced transparency in metamaterials. *Phys Rev Lett* 2008; **101**: 047401.
11 Biswas S, Duan J, Nepal D, Park K, Pachter R *et al.* Plasmon-induced transparency in the visible region via self-assembled gold nanorod heterodimers. *Nano Lett* 2013; **13**: 6287–6291.
12 Kildishev AV, Boltasseva A, Shalaev VM. Planar photonics with metasurfaces. *Science* 2013; **339**: 1232009.
13 Yu NF, Aieta F, Genevet P, Kats MA, Gaburro Z *et al.* A broadband, background-free quarter-wave plate based on plasmonic metasurfaces. *Nano Lett* 2012; **12**: 6328–6333.
14 Ni X, Emani NK, Kildishev AV, Boltasseva A, Shalaev VM. Broadband light bending with plasmonic nanoantennas. *Science* 2012; **335**: 427.
15 Sun SL, Yang K, Wang C, Juan T, Chen WT *et al.* High-efficiency broadband anomalous reflection by gradient meta-surfaces. *Nano Lett* 2012; **12**: 6223–6229.

doi:10.1038/lsa.2015.75

16 Chen P, Argyropoulos C, Alù A. Broadening the cloaking bandwidth with non-foster metasurfaces. *Phys Rev Lett* 2013; **111**: 233001.
17 Yin XB, Ye ZL, Rho J, Wang Y, Zhang X. Photonic spin hall effect at metasurfaces. *Science* 2013; **339**: 1405–1407.
18 Nikolaenko AE, De Angelis F, Boden S, Papasimakis N, Ashburn P *et al*. Carbon nanotubes in a photonic metamaterial. *Phys Rev Lett* 2010; **104**: 153902.
19 Zentgraf T, Christ A, Kuhl J, Giessen H. Tailoring the ultrafast dephasing of quasiparticles in metallic photonic crystals. *Phys Rev Lett* 2004; **93**: 243901.
20 Ren M, Jia B, Ou J, Plum E, Zhang J *et al*. Nanostructured plasmonic medium for terahertz bandwidth all-optical switching. *Adv Mater* 2011; **23**: 5540–5544.
21 Forati E, Hanson GW. Surface plasmon polaritons on soft-boundary graphene nanoribbons and their application in switching/demultiplexing. *Appl Phys Lett* 2013; **103**: 133104.
22 Liu N, Hentschel M, Weiss T, Alivisatos AP, Giessen H. Three-dimensional plasmon rulers. *Science* 2011; **332**: 1407–1410.
23 Yurista GL, Friesem AA. Very narrow spectral filters with multilayered grating-waveguide structures. *Appl Phys Lett* 2000; **77**: 1596–1598.
24 Davis TJ, Gómez DE, Vernon KC. Simple model for the hybridization of surface plasmon resonances in metallic nanoparticles. *Nano Lett* 2010; **10**: 2618–2625.
25 Zentgraf T, Christ A, Kuhl J, Gippius NA, Tikhodeev SG *et al*. Metallodielectric photonic crystal superlattices: Influence of periodic defects on transmission properties. *Phys Rev B* 2006; **73**: 115103.
26 Zentgraf T, Zhang S, Oulton RF, Zhang X. Ultranarrow coupling-induced transparency bands in hybrid plasmonic systems. *Phys Rev B* 2009; **80**: 195415.
27 Nau D, Schönhardt A, Bauer C, Christ A, Zentgraf T *et al*. Correlation effects in disordered metallic photonic crystal slabs. *Phys Rev Lett* 2007; **98**: 133902.
28 Zhao Y, Alù A. Tailoring the dispersion of plasmonic nanorods to realize broadband optical meta-waveplates. *Nano Lett* 2013; **13**: 1086–1091.
29 Tassin P, Zhang L, Zhao RK, Jain A, Koschny T *et al*. Electromagnetically induced transparency and absorption in metamaterials: the radiating two-oscillator model and its experimental confirmation. *Phys Rev Lett* 2012; **109**: 187401
30 Abi-Salloum TY. Electromagnetically induced transparency and Autler-Townes splitting: two similar but distinct phenomena in two categories of three-level atomic systems. *Phys Rev A* 2010; **81**: 053836.
31 Autler SH, Townes CH. Stark effect in rapidly varying fields. *Phys Rev* 1955; **100**: 703–722.
32 Liu H, Li B, Zheng L, Xu C, Zhang G *et al*. Multispectral plasmon-induced transparency in triangle and nanorod(s) hybrid nanostructures. *Opt Lett* 2013; **38**: 977–979.
33 Zhang FL, Zhao Q, Zhou J, Wang SX. Polarization and incidence insensitive dielectric electromagnetically induced transparency metamaterial. *Opt Express* 2013; **21**: 19675–19680.
34 Wang JQ, Yuan BH, Fan CZ, He JN, Ding P *et al*. A novel planar metamaterial design for electromagnetically induced transparency and slow light. *Opt Express* 2013; **21**: 25159–25166.
35 Zhang H, Virally S, Bao QL, Ping LK, Massar S *et al*. Z-scan measurement of the nonlinear refractive index of graphene. *Opt Lett* 2012; **37**: 1856–1858.
36 Li ZG, Yang JY, Wei T, Song YL. Intensive two-photon absorption induced decay pathway in a ZnO crystal: impact of light-induced defect state. *Appl Phys Lett* 2013; **103**: 252107.
37 Tucker RS, Ku PC, Chang-Hasnain CJ. Delay-bandwidth product and storage density in slow-light optical buffers. *Electron Lett* 2005; **41**: 208–209.
38 Dawlaty JM, Shivaraman S, Chandrashekhar M, Rana F, Spencer MG. Measurement of ultrafast carrier dynamics in epitaxial graphene. *Appl Phys Lett* 2008; **92**: 42116.
39 Del Fatti N, Voisin C, Achermann M, Tzortzakis S, Christofilos D *et al*. Nonequilibrium electron dynamics in noble metals. *Phys Rev B* 2000; **61**: 16956–16966.
40 Sasai J, Hirao K. Relaxation Behavior of nonlinear optical response in borate glasses containing gold nanoparticles. *J Appl Phys* 2001; **89**: 4548–4553.
41 Abb M, Albella P, Aizpurua J, Muskens OL. All-optical control of a single plasmonic nanoantenna–ITO hybrid. *Nano Lett* 2011; **11**: 2457–2463.
42 Henari FZ, Cazzini K, Akkari FE, Blau WJ. Beam waist changes in lithium niobate during *Z*-scan measurement. *J Appl Phys* 1995; **78**: 1373–1375.
43 Bristow AD, Rotenberg N, van Driel HM. Two-photon absorption and Kerr coefficients of silicon for 850–2200 nm. *Appl Phys Lett* 2007; **90**: 191104.
44 Ishikawa A, Tanaka T. Plasmon hybridization in graphene metamaterials. *Appl Phys Lett* 2013; **102**: 253110.

Supplementary information for this article can be found on the *Light: Science & Applications'* website (http://www.nature.com/lsa/).